Molecular hydrogen in Lyman alpha emitters

Livia Vallini,[1]* Pratika Dayal[2,3] and Andrea Ferrara[1]

[1]*Scuola Normale Superiore, Piazza dei Cavalieri 7, 56126 Pisa, Italy*
[2]*Institute for Astronomy, The University of Edinburgh, Royal Observatory, Blackford Hill, Edinburgh EH9 3HJ*
[3]*Leibniz Institute for Astrophysics, Potsdam, An der Sternwarte 16, Potsdam 14482, Germany*

ABSTRACT

We present a physically motivated model to estimate the molecular hydrogen (H_2) content of high-redshift ($z \approx 5.7$ and 6.6) Lyman α emitters (LAEs) extracted from a suite of cosmological simulations. We find that the H_2 mass fraction, f_{H_2}, depends on three main LAE physical properties: (a) star formation rate, (b) dust mass and (c) cold neutral gas mass. At $z \approx 5.7$, the value of f_{H_2} peaks and ranges between 0.5 and 0.9 for intermediate-mass LAEs with stellar mass $M_* \approx 10^9 - 10^{10} \, M_\odot$, decreasing for both smaller and larger galaxies. However, the largest value of the H_2 mass is found in the most luminous LAEs. These trends also hold at $z \approx 6.6$, although, due to a lower dust content, $f_{H_2}(z = 6.6) \approx 0.5 f_{H_2}(z = 5.7)$ when averaged over all LAEs; they arise due to the interplay between the H_2 formation/shielding controlled by dust and the intensity of the ultraviolet Lyman–Werner photodissociating radiation produced by stars. We then predict the carbon monoxide (CO) luminosities for such LAEs and check that they are consistent with the upper limits found by Wagg et al. for two $z > 6$ LAEs. At $z \approx 5.7$ and 6.6, the lowest CO rotational transition observable for both samples with the actual capabilities of the Atacama Large Millimeter Array (ALMA) is the CO(6$-$5). We find that at $z \approx 5.7$, about 1–2 per cent of LAEs, i.e. those with an observed Lyman α luminosity larger than $10^{43.2}$ erg s^{-1}, would be detectable with an integration time of 5–10 h (a signal-to-noise ratio of 5); at $z \approx 6.6$, none of the LAEs would be detectable in CO, even with an ALMA integration time of 10 h. We also build the CO 'flux function', i.e. the number density of LAEs as a function of the line-integrated CO flux, S_{CO}, and show that it peaks at $S_{CO} = 0.1$ mJy at $z = 5.7$, progressively shifting to lower values at higher redshifts. We end by discussing the model uncertainties.

Key words: ISM: clouds – ISM: molecules – galaxies: high-redshift – cosmology: theory – radio lines: galaxies – radio lines: ISM.

1 INTRODUCTION

The past few years have seen a rapid increase in the amount of data available on high-redshift galaxies. This has been made possible by a combination of state-of-the-art instruments such as the *Hubble Space Telescope*, the *Subaru* and *Keck* telescopes, and sophisticated selection techniques. Of the latter, one of the most successful approaches has been the use of the narrow-band technique (e.g. Malhotra et al. 2005; Kashikawa et al. 2006; Shimasaku et al. 2006; Hu et al. 2010) that is based on looking for the Lyman α (Lyα) emission at 1216 Å in the galaxy rest frame. Hundreds of such galaxies, called LAEs, have now been confirmed at $z \approx 2.25$ (Nilsson et al. 2009), $z \approx 3$ (Cowie & Hu 1998; Steidel et al. 2000; Matsuda et al. 2005; Venemans et al. 2007; Ouchi et al. 2008), $z \approx 4.5$ (Finkelstein

et al. 2007), $z \approx 5.7$ (Malhotra et al. 2005; Shimasaku et al. 2006), $z \approx 6.6$ (Taniguchi et al. 2005; Kashikawa et al. 2011) and $z \approx 7$ (Iye et al. 2006). Due to their large number statistics and unambiguous spectral signatures, LAEs are arguably the best probes of reionization and high-redshift galaxy evolution (Santos et al. 2004; Dijkstra, Lidz & Wyithe 2007; Kobayashi, Totani & Nagashima 2007, 2010; Dayal, Ferrara & Gallerani 2008; Dayal et al. 2009; Dayal, Ferrara & Saro 2010; Dayal & Ferrara 2011a).

However, using LAEs as probes of high-redshift galaxy populations, understanding them to study reionization and calculating their contribution to reionization requires an understanding of their star formation rates (SFRs). Translating the observed ultraviolet (UV) luminosity (1375 Å in the galaxy rest frame) into an intrinsic SFR is rendered hard by the fact that the continuum photons produced in a galaxy are attenuated by the dust in the galactic interstellar medium (ISM) before they reach the observer. Inferring the intrinsic SFR using the observed Lyα luminosity is even more complicated since

*E-mail: livia.vallini@sns.it

Lyα photons are absorbed both by the ISM dust and the neutral hydrogen (H I) in the intergalactic medium (IGM) along the line of sight between the emitter and the observer. Indeed, a number of studies point to LAEs being dust enriched, even at redshifts $z \approx 6$: using theoretical models, Dayal et al. (2010) have shown that at $z \approx 5.7$, the colour excess of LAEs, $E(B - V) \sim 0.15$ while, observationally, the colour excess values are in the range of $E(B - V) \approx 0.025$–0.32 at $z \approx 4$–5.7 (Lai et al. 2007; Pirzkal et al. 2007; Finkelstein et al. 2009). Furthermore, the observed Lyα luminosity depends both on the reionization state of the IGM and on the IGM peculiar velocities along the line of sight; inflows/outflows into/from a galaxy can blueshift/redshift the Lyα line, thereby decreasing/increasing the IGM Lyα transmission, T_α (Verhamme, Schaerer & Maselli 2006; Dayal & Ferrara 2011b; Dijkstra, Mesinger & Wyithe 2011). However, the extent to which peculiar velocities influence T_α is debatable since these calculations have mostly been performed under idealized situations. For example, Verhamme et al. (2006) have used spherically symmetric outflows of H I to show an enhancement in T_α; however, many studies, e.g. Fangano, Ferrara & Richter (2007) and references therein, have shown that Kelvin–Helmholtz instabilities would result in breaking up such symmetric outflows.

In this sense, H$_2$ is a far better indicator of the SFR since stars form in dense, cold molecular clouds (MCs); theoretical and observational constraints on the latter are then of utmost importance to shed light on the molecular content, and therefore the intrinsic SFR of these high-redshift galaxies. The H$_2$ content of galaxies is generally studied through observations of CO rotational emission lines (Solomon & Vanden Bout 2005; Omont 2007) that have been detected in more than a hundred high-redshift sources, even though searches for molecular gas at redshifts $z > 4$ have so far focused mainly on quasars and on the most massive, far-infrared-luminous and submillimetre galaxies (see Riechers 2011). As of now, only scant effort has been devoted to observing the molecular content of high-redshift ($z \geq 6$) LAEs. In one of the only observational works available, Wagg, Kanekar & Carilli (2009) have searched for low-J rotational CO emission lines in two LAEs at $z > 6.5$; the non-detection of any CO emission from these galaxies can then be used to put constraints on the amount of molecular gas in these sources.

In this work, our aim is to present a self-consistent and physically motivated model to calculate the H$_2$ fraction and mass, and relate it to the physical properties of the galaxies identified as LAEs at $z \approx 5.7$ and 6.6. To do so, we start by using a previously developed LAE model (see Dayal et al. 2008, 2009, 2010; Dayal & Ferrara 2011a), where these authors combined state-of-the-art cosmological smoothed particle hydrodynamics (SPH) simulations with a Lyα production/transmission model to successfully reproduce a large number of observational data sets. We couple this with a semi-analytic model that describes the structure of the MCs, to calculate the molecular hydrogen content taking into account its formation on dust grains, its destruction by UV photons and the shielding by H I in the ISM, as proposed by Krumholz, McKee & Tumlinson (2008, 2009) and McKee & Krumholz (2010). Once the molecular fraction is calculated for all of the LAEs at $z \approx 5.7$ and 6.6, we examine its correlations with the physical properties of the emitters, including the SFR, the total ISM dust mass and the amount of cold H I gas in the ISM. Translating the total H$_2$ mass into a CO luminosity, we compare the predictions of our model to the observations of Wagg et al. (2009). Finally, we estimate the time required to observe such CO emission with the Atacama Large Millimeter Array (ALMA), one of whose main goals is to observe molecular gas in high-z sources.

2 THE COSMOLOGICAL SIMULATIONS

In this section, we briefly describe the simulation used in this work and interested readers are referred to Tornatore et al. (2010) for a complete description. The simulation has been carried out using the TreePM-SPH code GADGET-2 (Springel 2005) with the implementation of chemodynamics as described in Tornatore et al. (2007). The adopted cosmological model corresponds to a Λ cold dark matter (ΛCDM Universe) with $\Omega_m = 0.26$, $\Omega_\Lambda = 0.74$, $\Omega_b = 0.0413$, $n_s = 0.95$, $H_0 = 73 \, \text{km s}^{-1} \, \text{Mpc}^{-1}$ and $\sigma_8 = 0.8$, thus consistent with the 5-year analysis of the *Wilkinson Microwave Anisotropy Probe* (*WMAP*) data (Komatsu et al. 2009). The simulation has a periodic box size of $75 \, h^{-1}$ comoving Mpc (cMpc) and contains 512^3 dark matter (DM) particles, and initially the same number of baryonic particles. The run assumes a uniform redshift-dependent UV background produced by quasars and galaxies, as given by Haardt & Madau (1996), and includes metallicity-dependent radiative cooling (Sutherland & Dopita 1993). The code has an effective model to describe star formation from a multi-phase ISM and a prescription for galactic winds triggered by supernova (SN) explosions (Springel & Hernquist 2003); the initial mass function (IMF) is taken to be Salpeter between $1 \text{and} 100 \, M_\odot$. Metals and energy are released by stars of different masses by properly accounting for mass-dependent lifetimes as proposed by Padovani & Matteucci (1993). The code uses the metallicity-dependent yields from Woosley & Weaver (1995); the yields for Type Ia supernovae (SNe Ia) and asymptotic giant branch (AGB) stars have been taken from van den Hoek & Groenewegen (1997).

Galaxies are identified as gravitationally bound groups of star particles by running a friends-of-friends (FOF) algorithm. Each FOF group is then decomposed into a set of disjoint substructures, which are identified as locally overdense regions in the density field of the background main halo by the SUBFIND algorithm (Springel, Yoshida & White 2001). After performing a gravitational unbinding procedure, only sub-haloes with at least 20 bound particles are considered to be genuine structures (Saro et al. 2006). For each galaxy in each of the snapshots of interest ($z \approx 5.7$ and 6.6), we obtain the total halo/gas/stellar mass ($M_h/M_g/M_*$), the SFR ($\dot{M}_*$), the mass-weighted gas/stellar metallicity (Z_g/Z_*), the mass-weighted age (t_*), the mass-weighted gas temperature and the half-mass radius of the dark matter halo.

2.1 Identifying LAEs

The simulated properties of each galaxy at $z \approx 5.7$ and 6.6 are used to calculate the total intrinsic Lyα (L_α^{int}) and continuum luminosity (L_c^{int}), which include both the contribution from stellar sources and from the cooling of collisionally excited H I in the ISM as shown in Dayal et al. (2010). To calculate the stellar contribution, we obtain the spectrum of each LAE using the population synthesis code STARBURST99 (Leitherer et al. 1999), using the simulated values of t_*, M_* and $\dot{M}_*$; the cooling radiation depends on the temperature of the ISM gas. The intrinsic Lyα luminosity can be translated into the observed luminosity such that $L_\alpha = L_\alpha^{int} f_\alpha T_\alpha$, while the observed continuum luminosity, L_c, is expressed as $L_c = L_c^{int} f_c$. Here, $f_\alpha (f_c)$ are the fractions of Lyα (continuum) photons escaping the galaxy, undamped by the ISM dust, and T_α is the fraction of the Lyα luminosity that is transmitted through the IGM, undamped by neutral hydrogen.

The main features of the model used to calculate f_c, f_α and T_α are: (a) for each galaxy the dust enrichment is derived by using

its intrinsic properties ($\dot{M}_*$, t_*, M_g) and assuming Type II super-novae (SNe II) to be the primary dust factories. The dust mass, M_d, is calculated including dust production due to SNe II, assuming an average dust mass produced per SN II of $0.5\,M_\odot$ (Todini & Ferrara 2001; Nozawa et al. 2003, 2007; Bianchi & Schneider 2007), dust destruction with an efficiency of about 40 per cent in the region shocked to speeds of $\geq 100\,\mathrm{km\,s^{-1}}$ by SN II shocks, assimilation of a homogeneous mixture of dust and gas into subsequent star formation (astration), and ejection of a homogeneous mixture of gas and dust from the galaxy due to SNe II; (b) the dust distribution radius, r_d, is taken to scale with the effective stellar distribution scale, r_e, such that $r_d \approx (0.6, 1.0)r_e$ at $z \approx (5.7, 6.6)$, respectively; the calculation of r_e is described later in Section 3.1; (c) f_c is calculated assuming a slab-like dust distribution and we use $f_\alpha = (1.5, 0.6)f_c$, as inferred for LAEs at $z \approx (5.7, 6.6)$; and (d) T_α is calculated using the mean photoionization rate predicted by the early reionization model (ERM; reionization ends at $z \approx 7$) as proposed by Gallerani et al. (2008), according to which the neutral hydrogen fraction of $\chi_{HI} = (6.0 \times 10^{-5},\ 2.3 \times 10^{-4})$ at $z \approx (5.7, 6.6)$.

Once the above calculations have been carried out, following the current observational criterion, galaxies with $L_\alpha \geq 10^{42.2}\,\mathrm{erg\,s^{-1}}$ and an observed Lyα equivalent width (EW) $= L_\alpha/L_c \geq 20$ Å are identified as LAEs. Complete details of these calculations can be found in Dayal et al. (2010) and Dayal & Ferrara (2011a).

3 MOLECULAR HYDROGEN PHYSICS

H_2 can be formed in galaxies by two main methods: the first, and rather inefficient method involves gas-phase reactions mainly through the coupled reactions $e^- + H \rightarrow H^- + h\nu$ and $H^- + H \rightarrow H_2 + e^-$ (McDowell 1961; Palla, Salpeter & Stahler 1983). The second, more efficient channel is through bond formation on dust grains: this process begins with the collision and absorption of at least two hydrogen atoms by the same dust grain. The hydrogen atoms are weakly bound to the grain surface through Van der Waals forces and can migrate on the grain either by tunnelling or by thermal hopping. If the hydrogen atoms encounter each other, bond formation takes place, the excess energy is released to the grain and the H_2 molecule is ejected into the gas phase (Gould, Gold & Salpeter 1963). However, H_2 molecules so produced can be dissociated by the far-ultraviolet (FUV) interstellar radiation field in the Lyman–Werner (LW) band between 11.2 and 13.6 eV; the twin processes of self-shielding and dust absorption (e.g. Hollenbach & Tielens 1999) drive the shielding of H_2 to FUV photons, thereby preventing photodissociation. Considering these processes is of utmost importance since H_2 is found in molecular clouds that are surrounded by a photodissociation region (PDR) where the gas is predominantly atomic.

In this work we estimate the H_2 mass of each LAE at $z \approx (5.7, 6.6)$ using the analytic model presented in Krumholz et al. (2008, 2009) and McKee & Krumholz (2010), hereafter referred to as the KMT model. In brief, the KMT model considers an idealized spherical cloud immersed in a uniform, isotropic LW radiation field. Then, the equations of radiative transfer coupled to the H_2 formation–dissociation balance are solved, assuming the cloud to be in the steady state.

The analytical solution to the H_2 mass fraction, $f_{H_2} = M_{H_2}/M_{HI}$, is then obtained by solving for the radial position at which the transition between the atomic envelope and the molecular interior occurs within the cloud; in this equation, M_{H_2} and M_{HI}, refer to

the mass of molecular hydrogen and the mass of neutral hydrogen respectively. The KMT study shows that the fraction of the radius at which this transition occurs is solely a function of the dust optical depth in the LW band and the dimensionless parameter χ, which are discussed in what follows.

3.1 Modelling molecular hydrogen in LAEs

We now describe the model used to calculate the H_2 content of the LAEs identified in the simulation snapshots at $z \approx 5.7$ and 6.6. We start by assuming that the MCs lie in a region that extends from the centre of the galaxy up to the effective stellar distribution radius, r_e, calculated in Dayal et al. (2010). This assumption has been motivated by the fact that star formation occurs in MCs; the physical distribution scale of MCs and the stars is therefore expected to be quite similar. Furthermore, the value of r_e is based on estimates following the results of Bolton et al. (2008), who have derived fitting formulae relating the V-band luminosity and the stellar distribution scale from their observations of massive, early-type galaxies between $z = 0.06$ and 0.36. Though not an entirely robust estimate, we extend this result to galaxies at $z \approx 5.7$ and 6.6 due to the paucity of observational data regarding the stellar distribution scales in high-redshift galaxies. However, such estimates are in surprisingly good agreement with recent observational results: Malhotra et al. (2011) find that the half-light radius of LAEs has a mean value of ≈ 0.16 arcsec at $z \approx 5.7$ and this remains constant for all redshifts in the range $2 \leq z \leq 6.5$; these estimates lie within 1σ of the mean value of the theoretical r_e estimates used throughout this paper.

As mentioned above, using the KMT model, the H_2 mass fraction solely depends on the dust optical depth in the LW band, τ_c, and the dimensionless parameter χ, such that the analytical solution for the H_2 fraction can be written as (McKee & Krumholz 2010)

$$f_{H_2} \simeq 1 - \left(\frac{3}{4}\right)\frac{s}{1 + 0.25s}, \tag{1}$$

where the dimensionless parameter s can be expressed as

$$s = \frac{\ln(1 + 0.6\chi + 0.01\chi^2)}{0.6\tau_c}. \tag{2}$$

Here,

$$\chi = \frac{f_{diss}E_0\sigma_d c}{n_{CNM}\mathcal{R}}, \tag{3}$$

where $f_{diss} \simeq 0.1$ (Draine & Bertoldi 1996) is the fraction of absorbed LW band photons that lead to dissociation of the H_2 molecules, E_0 is the free space photon number density in the LW band, σ_d is the dust absorption cross-section per hydrogen nucleus to LW photons, c is the speed of light, n_{CNM} is the number density of gas in the cold atomic medium that surrounds the molecular part of the cloud, and $\mathcal{R}$ is the coefficient for the rate of H_2 formation on the surface of dust grains.

It must be noted that these equations apply only for $s < 2$; for values of $s \geq 2$, the gas is predominantly atomic, such that $f_{H_2} = 0$. Also, we note that the calculations presented here concern only average quantities in a spherically symmetric framework; a full calculation of the radial dependence of the model parameters is the subject of ongoing work. We now explain the calculations of E_0, σ_d, n_{CNM}, $\mathcal{R}$ and τ_c in what follows.

3.1.1 LW photon number density

As mentioned in Section 2.1, we obtain the intrinsic spectrum of each LAE using the population synthesis code STARBURST99. Then, assuming all the stars to form at the centre of the galaxy, the number density of LW photons of a specific wavelength λ ($912 \leq \lambda \leq 1120$ Å), at a distance r from the centre, can be expressed as

$$n_\lambda(r) = \frac{L_\lambda}{4\pi c r^2} \left(\frac{\lambda}{hc} \right). \tag{4}$$

Here, L_λ is the monochromatic luminosity at the wavelength λ obtained using STARBURST99 and h is the Planck constant. The free space photon number density at radius r, in the entire LW band, n_{LW}, can then be calculated by integrating over all the wavelengths in the band such that

$$n_{LW}(r) = \frac{1}{4\pi r^2 c} \int_{912\text{Å}}^{1120\text{Å}} \frac{\lambda L_\lambda}{hc} d\lambda. \tag{5}$$

The value of n_{LW} averaged over a sphere of radius r_e then gives the photon number density in the LW band such that

$$E_0 \equiv \langle n_{LW} \rangle = 3 n_{LW}(r_e). \tag{6}$$

3.1.2 Cold neutral medium density

Much of the neutral gas in galaxies is observed to be cold, with temperatures of the order of $\sim$100 K (CNM), or warm, with temperatures of the order of $\sim$10^4 K (WNM), in approximate pressure balance (Wolfire et al. 2003); as pointed out before, MCs form in regions where the gas is primarily cold. To calculate the density of the cold neutral medium, we start by obtaining the fraction, f_4, of ISM gas with temperature $T \leq 10^4$ K (see also fig. 1, Dayal et al. 2010); the value of f_4 averaged over galaxies of different halo masses is shown in Table 1. However, the large volume simulated ($\approx$10^6 cMpc^3) naturally results in a low mass resolution, such that we are unable to resolve the cold and warm gas phases inside the ISM of individual galaxies. We therefore make the approximation that the ISM of each simulated galaxy has an equal amount of cold and warm neutral gas. The mass of the cold neutral gas, M_{CNM}, in any galaxy can then be calculated as

$$M_{CNM} = \frac{1}{2} f_4 M_H, \tag{7}$$

where $M_H = 0.76 M_{gas}$ is the mass of hydrogen in the ISM. We assume the gas to be distributed in a disc with a radius r_g and scale height H such that (Ferrara, Pettini & Shchekinov 2000)

$$r_g = 4.5 \lambda r_{200}, \tag{8}$$

Table 1. As a function of the halo mass range (column 1), we show the fraction of ISM gas with temperature $T \leq 10^4$ K (column 2).

M_h ($M_\odot$)	f_4
$<10^{10}$	0.58
$10^{10} - 10^{10.4}$	0.40
$10^{10.4} - 10^{10.8}$	0.35
$10^{10.8} - 10^{11.2}$	0.35
$>10^{11.2}$	0.35

$$\frac{H}{r_g} = 15.3 \lambda \left(\frac{c_s}{v_e} \right)^2. \tag{9}$$

Here, value of the spin parameter is taken to be $\lambda = 0.04$ (Ferrara et al. 2000) and the virial radius, r_{200}, is calculated assuming that the collapsed region has an overdensity of 200 times the critical density at the redshift considered. Assuming that the typical velocity that determines the scale height of the disc is that of WNM, the effective gas sound speed is taken to be $c_s = 10 \, \text{km s}^{-1}$. Finally, the halo escape velocity, v_e, is related to the circular velocity of the halo, v_c, by the relation $v_e = 2p v_c$ with $p = 1.65$ (Mac Low & Ferrara 1999). The average global number density of the CNM, n_{CNM}, can then be expressed as

$$n_{CNM} = \frac{M_{CNM}}{\pi r_g^2 H m_H}, \tag{10}$$

where m_H is the hydrogen mass.

3.1.3 Molecular hydrogen formation rate

The rate of H_2 formation on dust grains, $\mathcal{R}$, can be expressed as (Hirashita & Ferrara 2005)

$$\mathcal{R} = 4.1 \times 10^{-17} S \left(\frac{a}{0.1 \, \mu\text{m}} \right)^{-1} \left(\frac{\mathcal{D}}{10^{-2}} \right)$$
$$\times \left(\frac{T}{100 \, \text{K}} \right)^{1/2} \left(\frac{\delta}{2 \, \text{g cm}^{-3}} \right)^{-1} \text{cm}^3 \, \text{s}^{-1}, \tag{11}$$

where $S = S(T, T_d)$ is the sticking coefficient for hydrogen atoms on dust grains, T is the gas temperature, δ is the density of the dust grains, $\mathcal{D}$ is the dust-to-gas ratio, and a is the radius of the dust grain which is assumed to be a sphere. Following the assumptions of Dayal et al. (2010), we assume all the dust grains to be carbonaceous such that $\delta = 2 \, \text{g cm}^{-3}$; using the size distribution of dust grains produced by SNe II (Todini & Ferrara 2001), we use an average grain size value of $a = 300$ Å. As mentioned before, dust predominantly forms in high-density, cold MCs which have a more effective self-shielding to LW photons compared to the lower density WMN; following this argument, we use $T = 100$ K.

Furthermore, the sticking coefficient $S(T, T_d)$ is given by Hollenbach & McKee (1979) and Omukai (2000) as

$$S(T, T_d) = [1 + 0.04(T + T_d)^{0.5} + 2 \times 10^{-3} T + 8 \times 10^{-6} T^2]^{-1}$$
$$\times \{1 + \exp[7.5 \times 10^2 (1/75 - 1/T_d)]\}^{-1}, \tag{12}$$

where T_d is the dust temperature. However, the sticking coefficient is not affected by the exact dust temperature as long as $T_d \leq 70$ K, which is true for all LAEs, which have dust temperatures $T_d \approx$ 30–45 K.

3.1.4 Dust cross-section and optical depth

We now discuss the calculation of the dust cross-section per hydrogen atom to LW photons, which can be expressed as

$$\sigma_d = \frac{Q_{abs}(a) \pi a^2}{N_H}, \tag{13}$$

where $a = 300$ Å is the average radius of dust grains produced by SNe II as mentioned above, $Q_{abs}(a)$ is the effective cross-section normalized to the geometric one for the average grain size and a wavelength of 1000 Å corresponding to the centre of the LW band (Draine & Lee 1984) and N_H is the number of hydrogen nuclei per

dust grain. To calculate $N_{\rm H}$, we use the dust to gas ratio, $\mathcal{D}$ such that

$$\mathcal{D} = \frac{M_{\rm dust}}{M_{\rm gas}} \simeq \frac{\frac{4}{3}\pi a^3 \delta N_{\rm dust}}{\mu m_{\rm p} N_{\rm H}}, \tag{14}$$

where $\mu = 0.59$ is the mean molecular weight of a fully ionized gas of primordial composition. Substituting $N_{\rm H}$ from equation (13) into equation (14) yields

$$\sigma_{\rm d} = \frac{3}{4} \frac{\mu m_{\rm p} \mathcal{D}}{\delta} \frac{Q_{\rm abs}(a)}{a}. \tag{15}$$

From equations (11) and (15), we note that χ is independent of $\mathcal{D}$.

Finally, the dust optical depth in the LW band is calculated as

$$\tau_c = \frac{\Sigma_{\rm d} Q_{\rm abs}(a)}{\frac{4}{3} a \delta}, \tag{16}$$

where the dust surface density $\Sigma_{\rm d} = M_{\rm d}/(\pi r_{\rm d}^2)$ and $r_{\rm d} \approx (0.6, 1.0) \times r_{\rm e}$ at $z \approx (5.7, 6.6)$ as required to best fit the LAE UV luminosity functions (Dayal et al. 2010).

Once these calculations have been carried out, the total molecular hydrogen mass, $M_{\rm H_2}$, in each LAE is estimated as

$$M_{\rm H_2} = f_{\rm H_2} M_{\rm HI}, \tag{17}$$

where $M_{\rm HI} = f_4 M_{\rm H}$ is the neutral hydrogen mass in the gas disc within a radius $r_{\rm e}$ and scale height H, where star formation takes place.

4 RESULTS

Once the above calculations have been carried out, we can discuss the results regarding the molecular hydrogen fraction and the total H_2 mass, and relate these to the physical properties of LAEs at $z \approx$ 5.7 and 6.6. In what follows, we also calculate the visibility of such LAEs through their CO emission and end by making predictions for such detections in the ALMA Early Science Release (ESR).

4.1 Molecular hydrogen content of LAEs

As shown in Section 3.1, the H_2 fraction is decided by three important physical parameters: (a) the SFR which determines the intensity of the H_2-dissociating LW field, (b) the amount of cold gas available to shield the MC against the LW field and (c) the dust mass on which the H_2 forms, and which additionally shields the molecular hydrogen by absorbing LW photons. We now quantify how the molecular hydrogen fraction depends on each of these parameters.

We start our discussion by mentioning that the stellar mass of LAEs ranges between $M_* = 10^{8.0} - 10^{10.4} \, {\rm M_\odot}$ at $z \approx 5.7$. As expected in a hierarchical structure formation scenario where progressively larger objects form from the merger of smaller ones, such range narrows to $M_* \approx 10^{8.1} - 10^{10} \, {\rm M_\odot}$ at $z \approx 6.6$ (see also Table 2); galaxies with stellar masses above $10^{10} \, {\rm M_\odot}$ have not had
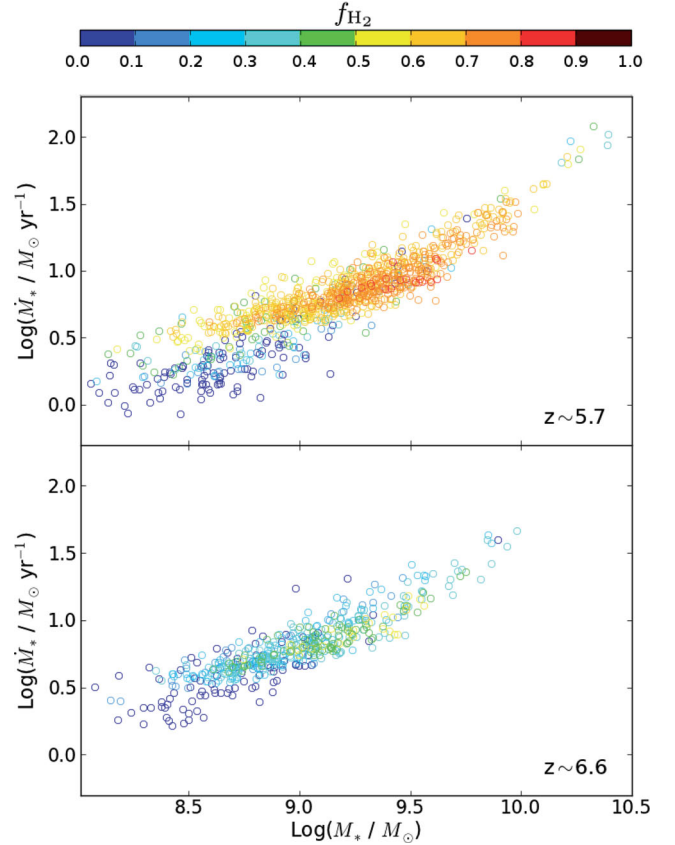

Figure 1. The molecular hydrogen fraction, $f_{\rm H_2}$, of LAEs at $z \approx 5.7$ (6.6) as a function of the stellar mass (M_*) and SFR ($\dot{M}_*$) is shown in the upper (lower) panels, respectively. Points are colour coded for different values of $f_{\rm H_2}$.

the time to assemble in large numbers by $z \approx 6.6$. Furthermore, the SFR of LAEs falls in the interval $\dot{M}_* \approx 0.8 - 120 \, {\rm M_\odot} \, {\rm yr}^{-1}$ at $z \approx 5.7$, with larger ($M_* \geq 10^{9.5} \, {\rm M_\odot}$) galaxies being the most efficient in star formation. At stellar masses lower than this value, the SFR–stellar mass relation flattens at both the redshifts considered, as seen from Fig. 1, due to the stronger effects of mechanical feedback (ejection of gas in outflows) inhibiting star formation (see Dayal et al. 2009). As a result of the narrower stellar mass range, the SFRs for $z \approx 6.6$ are concentrated in a narrower range between 1.6 and 46 ${\rm M_\odot} \, {\rm yr}^{-1}$ (see Table 2).

As for the molecular hydrogen fraction, starting with $z \approx 5.7$, we find $f_{\rm H_2} \leq 0.1$ for galaxies with $M_* < 10^9 \, {\rm M_\odot}$; it rises to $\approx 0.5 - 0.9$ for intermediate-mass galaxies with $M_* = 10^9 - 10^{10} \, {\rm M_\odot}$ and then decreases again to 0.2–0.6 for the few largest galaxies. Such behaviour can be explained as follows: although the smallest galaxies ($M_* < 10^9 \, {\rm M_\odot}$) have the smallest SFR (and hence weakest

Table 2. For all the LAEs at the redshifts shown (column 1), we show the range of stellar mass (column 2), the range of SFR (column 3), the range of cold neutral medium mass (column 4), the range of dust mass (column 5), the average molecular fraction (column 6), the average mass of molecular hydrogen (column 7), the average intrinsic CO(1−0) luminosity (column 8) and the average value of the CO(6−5) flux (column 9).

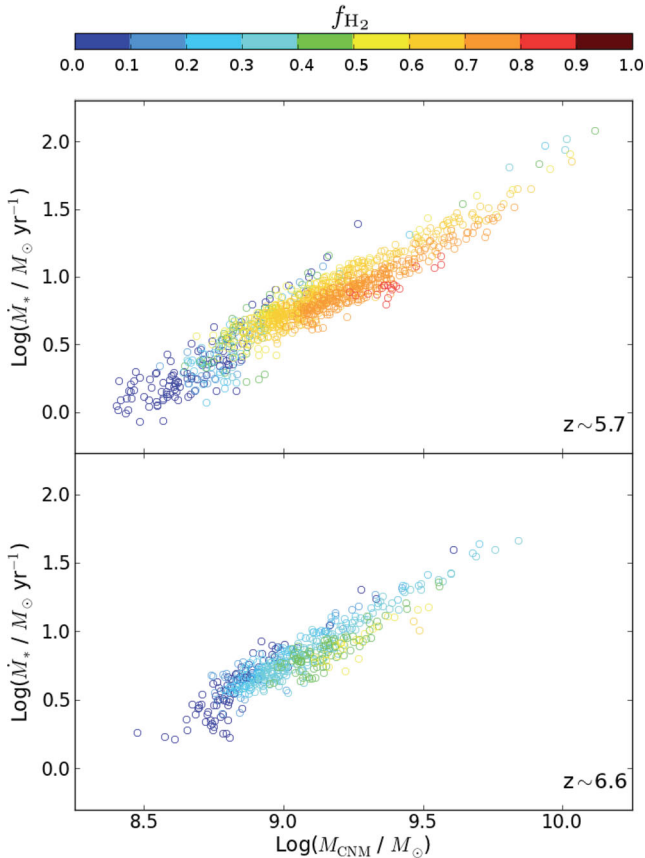| z	M_* $({\rm M_\odot})$	$\dot{M}_*$ $({\rm M_\odot}\,{\rm yr}^{-1})$	$M_{\rm CNM}$ $({\rm M_\odot})$	$M_{\rm d}$ $({\rm M_\odot})$	$\langle f_{\rm H_2} \rangle$	$\langle M_{\rm H_2} \rangle$ $({\rm M_\odot})$	$\langle L_{\rm CO} \rangle$ $({\rm K\,km\,s}^{-1}\,{\rm pc}^2)$	$\langle S_{\rm CO} \rangle$ (mJy)
5.7	$10^{8.0} - 10^{10.4}$	0.8–120	$10^{8.4} - 10^{10.1}$	$10^{3.4} - 10^{7.2}$	0.6	$10^{8.9}$	$10^{9.0}$	0.2
6.6	$10^{8.1} - 10^{10.0}$	1.6–46.4	$10^{8.5} - 10^{9.8}$	$10^{4.0} - 10^{6.9}$	0.3	$10^{8.4}$	$10^{8.5}$	0.06

Figure 2. The molecular hydrogen fraction, f_{H_2}, of LAEs at $z \approx 5.7$ (6.6) as a function of the stellar mass (M_*) and mass of cold H I ISM gas with temperature less than 100 K (M_{CNM}) is shown in the upper (lower) panels, respectively. Points are colour coded for different values of f_{H_2}.

Figure 3. The molecular hydrogen fraction, f_{H_2}, of LAEs at $z \approx 5.7$ (6.6) as a function of the stellar mass (M_*) and dust mass (M_d) is shown in the upper (lower) panels, respectively. Points are colour coded for different values of f_{H_2}.

LW field), they are also less dusty, resulting in a lower H_2 production rate and self-shielding ability against photodissociation. On the other hand, the larger SFR compared to the dust and cold gas mass in the largest galaxies leads to a decreased f_{H_2}. It is thus the intermediate-mass galaxies that show the largest H_2 fraction by virtue of a well-tuned balance between the H_2 formation and dissociation rates. Such an argument is supported by the fact that at a given value of the stellar mass, intermediate-mass galaxies with the lowest SFR have the largest H_2 fraction as seen from Fig. 1. Qualitatively, the situation remains the same at $z \approx 6.6$, although quantitatively, the f_{H_2} value is lower for all LAEs; the reason for this is detailed in what follows.

To understand the f_{H_2} dependence on the cold gas mass (M_{CNM}), we start by noting that M_{CNM} scales well with the SFR as shown in Fig. 2; more massive galaxies have a smaller cold mass fraction, possibly due to stellar sources heating a greater part of the ISM to higher temperatures (see also Table 1). From the same figure, we see that for a given value of M_{CNM}, galaxies with the lowest SFR have the largest value of f_{H_2}, which is easy to understand considering that for a given M_{CNM}, at lower SFR, the H_2 LW dissociation becomes less efficient. Again, it is the intermediate-mass galaxies that have the largest value of f_{H_2}, while the H_2 fraction is larger at $z \approx 5.7$ compared to $z \approx 6.6$ for all LAEs.

Dust also plays a key role in terms of the H_2 abundance since this molecule predominantly forms on dust grains which also shield the molecular hydrogen so formed, by absorbing LW photons. The dust mass for each LAE has been calculated as explained in Section 2.1;
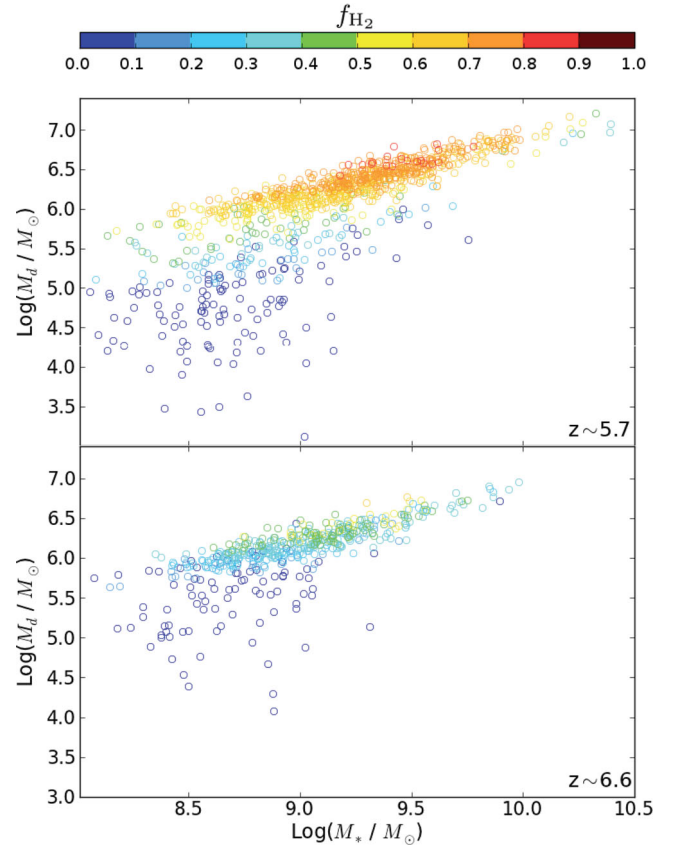
since we assume stellar sources (i.e. SNe II) to be the main dust producers, the total dust mass scales well with the stellar mass, ranging between $10^{3.4}$ and $10^{7.2}$ M$_\odot$ at $z \approx 5.7$. As mentioned before, since H_2 forms on dust grains, naively it might be expected that the larger the dust content, the larger is the value of f_{H_2}. However, this does not hold true; the LW intensity in the largest galaxies is enough to dissociate the H_2 formed as a result of which, the intermediate-mass galaxies end up with the largest H_2 fraction. As expected, at a given value of M_*, galaxies with the largest dust mass have the largest f_{H_2} value (Fig. 3).

Finally, we discuss why the value of f_{H_2} is lower at $z \approx 6.6$ compared to $z \approx 5.7$, even though galaxies identified as LAEs are extremely similar at these redshifts, in terms of M_*, $\dot{M}_*$, M_d and M_{CNM} (see Table 2): as mentioned in Section 3.1.4, the value of the dust distribution radius, $r_d = (0.6, 1.0)r_e$ at $z \approx (5.7, 6.6)$, is fixed by matching the observed LAE UV luminosity functions. These values imply that the dust is more concentrated in the inner parts of LAEs than the stars themselves, perhaps hinting at the existence of dust/metallicity radial gradients. We note that r_e, the stellar distribution scale, is similar at both the redshifts considered. The larger value of r_d results in a dust optical depth that is about 1.6 times smaller at $z \approx 6.6$ as compared to that 5.7 (see equation 16); although comparable H_2 masses would be produced in LAEs with similar physical properties at both $z \approx 5.7$ and 6.6, a larger amount is dissociated at $z \approx 6.6$ due to a decreased dust absorption of H_2-dissociating LW photons. Averaged over all LAEs, $f_{H_2} \approx 0.6$ at $z \approx 5.7$, and only $f_{H_2} \approx 0.3$ at $z \approx 6.6$, as seen from Fig. 4 and Table 2.
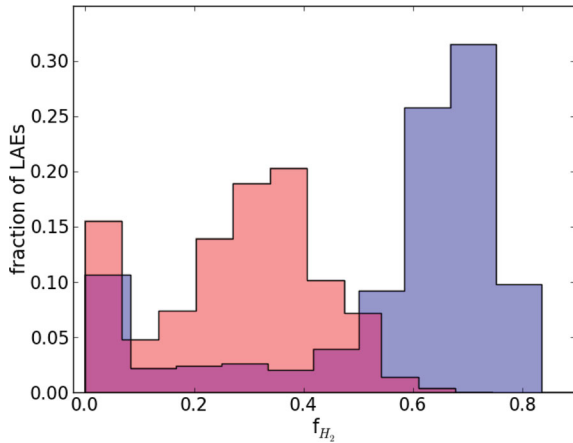
Figure 4. Normalized distribution of the number of LAEs as a function of the molecular hydrogen fraction f_{H_2} at $z \approx 5.7$ (dark/blue) and $z \approx 6.6$ (light/red).

From the same figure, we see that while f_{H_2} covers the broad range $0-0.85$ at $z \approx 5.7$, no LAEs have $f_{H_2} \geq 0.65$ at $z \approx 6.6$, as a result of the smaller dust optical depth. Finally, translating the value of f_{H_2} into a total M_{H_2} (equation 17), we find the average value of $M_{H_2} \approx 10^{8.9}$ and $10^{8.4}$ at $z \approx 5.7$ and 6.6, respectively, as shown in Table 2.

To summarize, we find that intermediate-mass LAEs ($M_* \approx 10^9 - 10^{10}\,\mathrm{M_\odot}$) have the largest molecular hydrogen fraction; a delicate balance between $\dot{M}_*$, M_{CNM} and M_d leads to H_2 formation (and self-shielding) dominating over H_2 photodissociation. Finally, due to a smaller dust optical depth (by a factor of ≈ 1.6) at $z \approx 6.6$, the H_2 fraction is about twice as large at $z \approx 5.7$ for LAEs with comparable physical properties.

4.2 CO detectability in LAEs

Now that the dependence of f_{H_2} on the physical properties of LAEs has been understood, we are in a position to make predictions for the H_2 detectability in these galaxies. H_2 has strongly forbidden rotational transitions; the rotational–vibrational lines have very high excitation temperatures, that are attainable only under somewhat extreme conditions involving intense irradiation or shock waves (see Solomon & Vanden Bout 2005) in the absence of which the H_2 is invisible. On the other hand, CO has a weak dipole moment: its rotational levels are then easily excited and thermalized by collisions with H_2. In addition, CO is a very stable molecule and the most abundant after H_2 (e.g. Solomon & Vanden Bout 2005; Omont 2007). Because of such considerations, it is popularly used as a tracer of H_2.

The luminosity of the CO(1$-$0) transition can be related to M_{H_2} mass as

$$L_{CO} = M_{H_2}/\alpha. \tag{18}$$

The parameter α used in the equation above depends on the distribution of star-forming clouds: in the Milky Way, where star formation takes place in molecular clouds with dense cores, confined by self-gravity, $\alpha = 4.6\,\mathrm{M_\odot\,K\,km\,s^{-1}\,pc^2}$ (Solomon et al. 1987). On the other hand, in high-redshift Ultra Luminous Infrared Galaxies (ULIRGs), where star formation is expected to occur in a dense intercloud medium bound by the potential of the galaxy, α has a much lower value of $0.8\,\mathrm{M_\odot\,K\,km\,s^{-1}\,pc^2}$ (Downes & Solomon 1998). It is worth noting that the value of α is also related to the
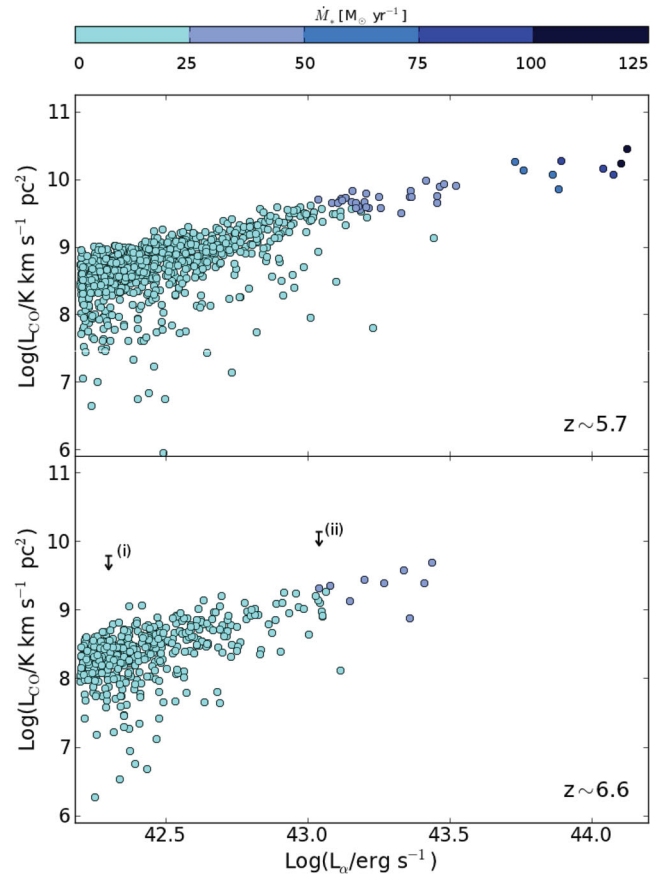

Figure 5. As a function of the observed Lyα luminosity (L_α), we show the estimated CO luminosity at $z \approx 5.7$ and 6.6 in the upper and lower panels, respectively; the points shown are colour coded according to the SFR. In the lower panel, the arrows indicate the upper limit on L_{CO} obtained by Wagg et al. (2009): (i) corresponds to the non-detection of the CO(1$-$0) line of HCM 6A, an LAE at $z \approx 6.6$, with SFR $\approx 2\,\mathrm{M_\odot\,yr^{-1}}$ (Hu et al. 2002). (ii) corresponds to the non-detection of the CO(1$-$0) line of IOK-1, a $z \approx 7$ LAE with SFR $\approx 10\,\mathrm{M_\odot\,yr^{-1}}$ (Iye et al. 2006).

metallicity of the interstellar gas (e.g. Leroy et al. 2009; Narayanan et al. 2011; Genzel et al. 2012). Using the Green Bank Telescope, Wagg et al. (2009) undertook a search for CO emission in two LAEs at $z > 6$, and they adopted the ULIRG value of the conversion factor to estimate M_{H_2}. For a reasonable comparison with such LAE data, we use the same value of $\alpha = 0.8\,\mathrm{M_\odot\,K\,km\,s^{-1}\,pc^2}$ to compute the CO(1$-$0) luminosity values for simulated LAEs at $z \approx (5.7, 6.6)$. We find that the value of L_{CO} scales with L_α for both the redshifts considered as shown in Fig. 5; quantitatively, we find $L_{CO} \propto L_\alpha^{(1.04, 1.07)}$ at $z \approx (5.7, 6.6)$, respectively. Although such a relation has a huge scatter, this implies that the brightest LAEs are the best candidates for molecular emission searches.

Interestingly, such a trend also implies that although the value of f_{H_2} is the largest for the intermediate mass/luminosity LAEs (see Section 4.1), the increasingly large neutral hydrogen mass, M_{HI}, in the star-forming disc (see equation 17) of massive galaxies wipes out such a subtle signature, whose imprint remains as a flattening of the $L_{CO}-L_\alpha$ relation towards the most luminous objects. As expected, as a result of their lower dust optical depth, and hence, a lower molecular hydrogen fraction, the CO luminosity for LAEs is smaller at $z \approx 6.6$ than that at $z \approx 5.7$; averaged over all LAEs, the CO luminosity at $z \approx 6.6$ is about a factor of 3 lower than that at $z \approx 5.7$, as shown in Table 2. As a validation of our model, our

theoretical L_{CO} estimates are in accord with the upper limits found by Wagg et al. (2009) for their observed LAEs, as seen from the lower panel of Fig. 5, which represents an encouraging sanity check of our model. Finally, we note that α is expected to be larger than the Galactic value in low-metallicity environments (Leroy et al. 2009; Narayanan et al. 2011; Genzel et al. 2012), which is likely the case for LAEs, while we have used a value derived using ULIRGs. As expected, an increase in the value of α would lead to a decrease in the CO luminosity, thereby negatively affecting the CO detectability of LAEs.

4.3 Predictions for ALMA early science

Now that the CO(1−0) luminosity has been calculated for all LAEs in our simulation, we make predictions for the detectability of such CO lines using ALMA. As of now, these observations have been limited to the most luminous high-z sources such as QSOs (e.g. Cox et al. 2002; Bertoldi et al. 2003; Walter et al. 2004; Weiß et al. 2007; Wang et al. 2010; Riechers et al. 2011) and submillimetre galaxies (SMGs; e.g. Greve et al. 2005; Tacconi et al. 2006); normal galaxies such as Lyman-break galaxies (LBGs) have only been detected at a much lower redshift, $z \approx 3$. We start by noting that ALMA Early Science (Cycle 0) consists of the use of 16 antennas and a limited number of bands. In this configuration, the lowest CO rotational transition observable at $z \approx 5.7$ is CO(5−4) ($\nu_{rest} = 576.267$ GHz), which falls within ALMA Band 3 (84–116 GHz). However, as shown in what follows, the rotational transition strength of the CO(5−4) line is quite comparable to that of CO(6−5). The latter is the lowest line observable with the ALMA Cycle 0 for both ($z \approx 5.7$ and 6.6) samples, for which reason we show results for the CO(6−5) transition in what follows; in the future, using the full capabilities of ALMA, lower frequency bands (31.3–45 GHz and 67–90 GHz) will also allow for the study of lower-J CO line transitions at high redshift.

We now describe how we translate the CO(1−0) luminosities calculated above in Section 4.2 in to CO(6−5) luminosities. Theoretical fits to observational CO spectral energy distributions (SEDs) have been carried out by several authors using local thermal equilibrium (LTE; Obreschkow et al. 2009) or large velocity gradient (LVG) models (Bayet et al. 2009) to describe the molecular gas. We use the model proposed by Obreschkow et al. (2009), which assumes a single gas component in LTE. In this framework, the frequency-integrated luminosity from the transition ($J \rightarrow J - 1$) can be expressed as (Obreschkow et al. 2009)

$$L(J \rightarrow J - 1) \propto 1 - \exp(\tau_J)\frac{J^4}{\exp(\frac{h\nu_{CO}J}{k_b T_e}) - 1}, \tag{19}$$

where $T_e = 100$ K is the gas excitation temperature, $\nu_{CO} = 115.271$ GHz is the rest-frame frequency of the CO(1−0) transition, τ_J is the optical depth and k_b is the Boltzmann constant. Furthermore, τ_J can be expressed as

$$\tau_J = 7.2\bar{\tau}\exp(-\frac{h\nu_{CO}J^2}{2k_b T_e})\sinh\left(\frac{h\nu_{CO}J}{2k_b T_e}\right), \tag{20}$$

where $\bar{\tau}$ is an experimentally determined normalization constant, which we take to be $\bar{\tau} = 2$, following the results of Obreschkow et al. (2009).

Considering that the frequency of the ($J \rightarrow J - 1$) transition is related to that of (1−0) by $\nu_J = J\nu_{CO}$, and using the relation between frequency-integrated luminosity L and the brightness temperature
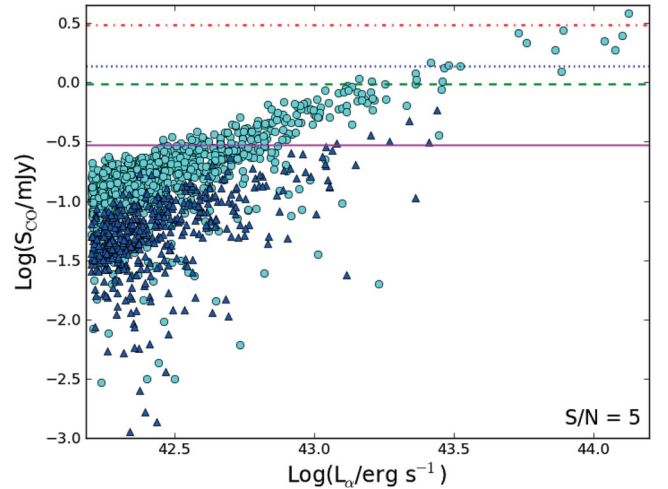
Figure 6. The line-integrated CO(6−5) flux, S_{CO}, as a function of L_α observed for LAEs at $z \approx 5.7$ (circles) and $z \approx 6.6$ (triangles). Horizontal lines represent the ALMA Cycle 0 sensitivity for an S/N of 5, for an integration time of 1 h (dot–dashed line), 5 h (dotted line) and 10 h (dashed line), assuming a spectral resolution of 50 km s^{-1}. The solid line represents the sensitivity (S/N = 5) achieved with 10 h of integration time with 50 antennas.

luminosity L_{CO} (cf. appendix A in Obreschkow et al. 2009):

$$L_{CO} = (8\pi k_b)^{-1}\lambda_e^3 L = (8\pi k_b)^{-1}\left(\frac{c}{\nu_e}\right)^3 L, \tag{21}$$

we obtain the $L_{CO}(6-5)$ luminosity in units of (K km s^{-1} pc^2) and find that $L_{CO}(6-5) = 1.58 L_{CO}(1-0)$, while $L_{CO}(5-4) = 1.75 L_{CO}(1-0)$; all the results presented for the CO(6−5) transition also remain largely valid for the CO(5−4) transition.

This line luminosity can be converted into the line-integrated flux, S_{CO}, such that

$$L_{CO} = 3.25 \times 10^7 S_{CO}\Delta V \nu_{obs}^{-2}(1 + z)^{-3} D_L^2, \tag{22}$$

where $S_{CO}\Delta V \equiv S^V$ is the velocity-integrated flux (Jy km s^{-1}), ν_{obs} is the observed frequency in GHz and D_L is the luminosity distance. We then assume that the CO(6−5) line has a Gaussian profile with a width given by the rotational velocity of the galaxy, ν_r, which we take to be equal to 1.5 times the halo rotation velocity (see Dayal et al. 2009). The average value of ν_r for LAEs at both the redshifts considered is of the order of 200 km s^{-1}. The observable CO flux S_{CO} can then be expressed as $S_{CO} \simeq S^V/\nu_r$.

As noted in Section 4.2, the CO(1−0) luminosity value scales with the observed Lyα luminosity; the line-integrated flux is therefore also expected to behave in a similar way. This is indeed the case, as seen from Fig. 6. Albeit with a large scatter, galaxies with the largest Lyα luminosity show the largest value of $S_{CO}(6-5)$ at both $z \approx 5.7$ and 6.6; as expected from a comparison of the CO(1−0) luminosities, the average value of S_{CO} is about three times lower at $z \approx 6.6$, compared to $z \approx 5.7$ (Table 2). We find that at $z \approx 6.6$, none of the LAEs would be detectable in CO, even with an ALMA Cycle 0 integration time for about 10 h. On the other hand, at $z \sim 5.7$, about 1–2 per cent of LAEs, i.e. those with $L_\alpha \geq 10^{43.2}$ erg s^{-1}, could be detectable with an ALMA integration time of 5–10 h (i.e. a detection limit of $\sim$1–1.4 mJy, respectively), assuming a signal-to-noise ratio (S/N) of 5. However, using 50 antennas of ALMA with an integration time of 10 h increases the sensitivity to about 0.3 mJy, making a significant change such that about 13 and 1.4 per cent of LAEs become detectable at $z \approx 5.7$ and 6.6, respectively.
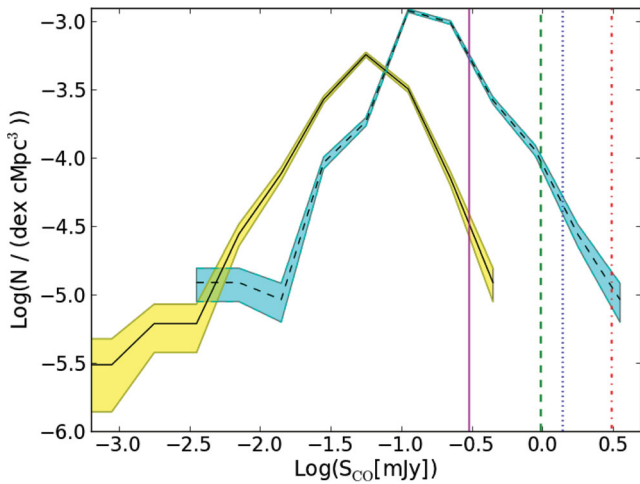
Figure 7. The number density of LAEs at $z \approx 5.7$ and 6.6 is shown as a function of the line-integrated CO(6−5) flux using dashed and solid lines, respectively; shaded regions show the Poissonian errors. Vertical dot–dashed, dotted and dashed lines represent the ALMA sensitivity limits for 16 antennas assuming an S/N of 5, for an integration time of 1, 5 and 10 h, respectively. The vertical solid line represents the sensitivity (S/N = 5) achieved with 10 h of integration time with 50 antennas.

To clarify such results, we present the CO 'flux function' (see Fig. 7), i.e. the number density of LAEs as a function of the line-integrated CO flux, $S_{CO}(6−5)$. As clearly seen again, none of the $z \approx 6.6$ LAEs is detectable with the Cycle 0 of ALMA, even for a 10-h detection limit of about 1 mJy. On the other hand, the $z \approx 5.7$ flux function extends into the 1–10 ALMA detection bands as mentioned above. However, the peak of the function lies at $S_{CO} \approx 0.1$ mJy at $z \approx 5.7$; due to the lower H_2 mass at $z \approx 6.6$, the flux function peaks at a lower value of about 0.06 mJy. As mentioned above, using 50 ALMA antennas for an integration time of 10 h increases the number of LAEs detectable in CO; as expected, this leads to a larger part of the 'flux function' being observed at both the redshifts considered.

5 SUMMARY AND CONCLUSIONS

Using a physically motivated model, we present results concerning the H_2 fraction and the total H_2 mass inside the ISM of LAEs at $z \approx 5.7$ and 6.6 by coupling a semi-analytic model of the molecular content of galaxies to a previously developed LAE model that reproduces a number of observed LAE data sets.

We start by using cosmological SPH simulations to obtain the physical properties of each simulated galaxy, including the total halo/gas/stellar mass ($M_h/M_g/M_*$), the SFR ($\dot{M}_*$), the mass-weighted gas/stellar metallicity (Z_g/Z_*), the mass-weighted age (t_*) and the mass-weighted gas temperature; the values of Z_*, t_* and $\dot{M}_*$ of each galaxy are then used to produce its intrinsic spectrum using STARBURST99 (Leitherer et al. 1999). Assuming SNe II to be the primary sources of dust, we calculate the ISM dust attenuation of both Lyα and continuum photons, and the IGM Lyα transmission, to select galaxies as LAEs (Dayal et al. 2009, 2010; Dayal & Ferrara 2011b). For each of these galaxies, the value of f_{H_2} is calculated using the analytic model proposed by Krumholz et al. (2008, 2009) and McKee & Krumholz (2010), which considers an idealized spherical molecular cloud immersed in a uniform and isotropic H_2-dissociating Lyman–Werner radiation field; under approximations of steady state, the value of f_{H_2} is solely a function of the

dust optical depth to LW photons, and a dimensionless parameter, χ. The latter depends on: (a) the intensity of the LW field which is determined by $\dot{M}_*$; (b) the total dust mass, M_d, which both enables H_2 formation on the surface of dust grains and shields the H_2 to LW photons; and (c) the cold H I mass, M_{CNM}, providing the key ingredient to produce H_2.

Using this model, we find that at $z \approx 5.7$, the value of f_{H_2} peaks and ranges between 0.5 and 0.9 for intermediate-mass LAEs with $M_* \approx 10^9−10^{10}$ M$_{\odot}$, decreasing for both smaller and larger galaxies; this trend also holds at $z \approx 6.6$. Such behaviour can be explained as follows: compared to intermediate-mass galaxies, smaller galaxies have smaller SFR (and hence a lower value of the dissociating LW field), lower dust masses for forming H_2 and a lower cold gas (and dust) mass for self-shielding the H_2 so formed against the dissociating LW field; on the other hand, the larger SFR compared to the dust and cold gas mass in the largest galaxies leads to a lower f_{H_2}. Such an argument is validated by the fact that at a given stellar mass, galaxies with the lowest SFR, largest cold gas mass and largest dust mass have the largest value of f_{H_2}. Furthermore, we find that for LAEs with comparable SFR/gas mass/dust masses, f_{H_2} is about twice as large at $z \approx 5.7$ than at 6.6; to reproduce the LAE UV luminosity function data, the dust distribution radius at $z \approx 6.6$ is about 1.6 times larger than that at 5.7, for similar LAE properties. As a result, the dust optical depth to LW photons is lower at $z \approx 6.6$, which leads to a larger amount of H_2 being dissociated.

We then translate the H_2 mass we obtain into a CO luminosity. Recently, Wagg et al. (2009) used the Green Bank Telescope to look for CO emission in two LAEs at $z > 6$, both of which resulted in non-detections. To compare our model predictions to their observations, we used a value of $\alpha = 0.8$ M$_{\odot}$ K km s^{-1} pc^2 to translate the H_2 mass into a CO(1−0) luminosity, L_{CO}. We find that the value of L_{CO} scales with L_{α}, for both the redshifts considered; although the value of f_{H_2} is the largest for the intermediate mass/luminosity LAEs (see Section 4.1), the increasingly large neutral hydrogen mass, M_{HI}, in the star-forming disc of increasingly massive galaxies wipes out such a subtle signature. This result also implies that the brightest LAEs are the best candidates for molecular emission searches. As a reasonable validation of our model, our theoretical L_{CO} estimates are in accord with the upper limits found by Wagg et al. (2009) in their experimental work.

At $z \approx 5.7$ and 6.6, the lowest CO rotational transition observable with ALMA is the CO(6−5). We find that at $z \approx 5.7$, about 1–2 per cent of the LAEs, i.e. those with $L_{\alpha} \geq 10^{43.2}$ erg s^{-1}, could be detectable with an integration time of 5–10 h, respectively, assuming an S/N of 5. Our results at $z \approx 6.6$ are more pessimistic; none of the LAEs would be detectable in CO, even with an ALMA integration time of about 10 h. We also present the CO 'flux function', the number density of LAEs as a function of S_{CO} where we show that the number density of objects peaks at a value of about 0.1 mJy, which is much beyond the sensitivity of ALMA; this peak shifts to progressively lower values with increasing redshift.

Finally, we discuss the main caveats in the model. First, the calculations presented here concern only average quantities in a spherically symmetric framework and a full calculation of the radial dependence of f_{H_2} is the subject of an ongoing work. Secondly, the dust masses used in this work have been calculated assuming SNe II to be the primary sources of dust production, which is a reasonable assumption given that a number of authors (Todini & Ferrara 2001; Dwek, Galliano & Jones 2007) have shown that the contribution of AGB stars becomes progressively less important and at some point negligible towards higher redshifts ($z \gtrsim 5.7$) when the Universe is less than 1-Gyr old. However, it must be

noted that under certain conditions thought to hold in quasars, in which extremely massive starbursts occur, the contribution of AGB can become important somewhat earlier (see Valiante et al. 2009). Thirdly, the stellar distribution scale (and radial extent of the MC) is based on estimates following the results of Bolton et al. (2008), who have derived fitting formulae relating the V-band luminosity and the stellar distribution scale from their observations of massive, early-type galaxies between $z = 0.06$ and 0.36; however, we note that such estimates are in surprisingly good agreement (to within 1σ) with recent observational results of $z \approx 5.7$ LAEs (Malhotra et al. 2011). Fourthly, the large cosmological volume simulated naturally results in a low mass resolution, such that we are unable to resolve density and temperature of the gas in the interior of individual galaxies. We have therefore estimated the ISM gas temperature distribution over broad halo mass bins. Furthermore, in our calculations, we have assumed that half of the gas mass with temperatures of $T < 10^4$ K is cold, with $T < 100$ K. Finally, we have used a ULIRG value for the factor α, used to translate the H$_2$ mass into a CO luminosity. However, this parameter depends on a number of poorly known properties of high-z galaxies, such as the spatial/mass distribution of their MCs and the gas metallicity (Leroy et al. 2009; Narayanan et al. 2011; Genzel et al. 2012). It is hoped that upcoming data from state-of-the-art instruments such as ALMA will be able to shed light and clarify such thorny issues.

REFERENCES

Bayet E., Gerin M., Phillips T. G., Contursi A., 2009, MNRAS, 399, 264
Bertoldi F. et al., 2003, A&A, 409, L47
Bianchi S., Schneider R., 2007, MNRAS, 378, 973
Bolton A. S., Treu T., Koopmans L. V. E., Gavazzi R., Moustakas L. A., Burles S., Schlegel D. J., Wayth R., 2008, ApJ, 684, 248
Cowie L. L., Hu E. M., 1998, AJ, 115, 1319
Cox P. et al., 2002, A&A, 387, 406
Dayal P., Ferrara A., 2011a, MNRAS, 417, L41
Dayal P., Ferrara A., 2011b, ArXiv e-prints
Dayal P., Ferrara A., Gallerani S., 2008, MNRAS, 389, 1683
Dayal P., Ferrara A., Saro A., Salvaterra R., Borgani S., Tornatore L., 2009, MNRAS, 400, 2000
Dayal P., Ferrara A., Saro A., 2010, MNRAS, 402, 1449
Dijkstra M., Lidz A., Wyithe J. S. B., 2007, MNRAS, 377, 1175
Dijkstra M., Mesinger A., Wyithe J. S. B., 2011, MNRAS, 414, 2139
Downes D., Solomon P. M., 1998, ApJ, 507, 615
Draine B. T., Bertoldi F., 1996, ApJ, 468, 269
Draine B. T., Lee H. M., 1984, ApJ, 285, 89
Dwek E., Galliano F., Jones A. P., 2007, Nuovo Cimento, 122, 959
Fangano A. P. M., Ferrara A., Richter P., 2007, MNRAS, 381, 469
Ferrara A., Pettini M., Shchekinov Y., 2000, MNRAS, 319, 539
Finkelstein S. L., Rhoads J. E., Malhotra S., Pirzkal N., Wang J., 2007, ApJ, 660, 1023
Finkelstein S. L., Rhoads J. E., Malhotra S., Grogin N., 2009, ApJ, 691, 465
Gallerani S., Ferrara A., Fan X., Choudhury T. R., 2008, MNRAS, 386, 359
Genzel R. et al., 2012, ApJ, 746, 69
Gould R. J., Gold T., Salpeter E. E., 1963, ApJ, 138, 408
Greve T. R. et al., 2005, MNRAS, 359, 1165
Haardt F., Madau P., 1996, ApJ, 461, 20

Hirashita H., Ferrara A., 2005, MNRAS, 356, 1529
Hollenbach D., McKee C. F., 1979, ApJS, 41, 555
Hollenbach D. J., Tielens A. G. G. M., 1999, Rev. Mod. Phys., 71, 173
Hu E. M., Cowie L. L., McMahon R. G., Capak P., Iwamuro F., Kneib J.-P., Maihara T., Motohara K., 2002, ApJ, 568, L75
Hu E. M., Cowie L. L., Barger A. J., Capak P., Kakazu Y., Trouille L., 2010, ApJ, 725, 394
Iye M. et al., 2006, Nat, 443, 186
Kashikawa N. et al., 2006, ApJ, 648, 7
Kashikawa N. et al., 2011, ApJ, 734, 119
Kobayashi M. A. R., Totani T., Nagashima M., 2007, ApJ, 670, 919
Kobayashi M. A. R., Totani T., Nagashima M., 2010, ApJ, 708, 1119
Komatsu E. et al., 2009, ApJS, 180, 330
Krumholz M. R., McKee C. F., Tumlinson J., 2008, ApJ, 689, 865
Krumholz M. R., McKee C. F., Tumlinson J., 2009, ApJ, 693, 216
Lai K., Huang J.-S., Fazio G., Cowie L. L., Hu E. M., Kakazu Y., 2007, ApJ, 655, 704
Leitherer C. et al., 1999, ApJS, 123, 3
Leroy A. K. et al., 2009, ApJ, 702, 352
Mac Low M.-M., Ferrara A., 1999, ApJ, 513, 142
Malhotra S. et al., 2005, ApJ, 626, 666
Malhotra S., Rhoads J. E., Finkelstein S. L., Hathi N., Nilsson K., McLinden E., Pirzkal N., 2011, ArXiv e-prints
Matsuda Y. et al., 2005, ApJ, 634, L125
McDowell M. R. C., 1961, Observatory, 81, 240
McKee C. F., Krumholz M. R., 2010, ApJ, 709, 308
Narayanan D., Krumholz M., Ostriker E. C., Hernquist L., 2011, MNRAS, 418, 664
Nilsson K. K., Tapken C., Møller P., Freudling W., Fynbo J. P. U., Meisenheimer K., Laursen P., Östlin G., 2009, A&A, 498, 13
Nozawa T., Kozasa T., Umeda H., Maeda K., Nomoto K., 2003, ApJ, 598, 785
Nozawa T., Kozasa T., Habe A., Dwek E., Umeda H., Tominaga N., Maeda K., Nomoto K., 2007, ApJ, 666, 955
Obreschkow D., Heywood I., Klöckner H.-R., Rawlings S., 2009, ApJ, 702, 1321
Omont A., 2007, Rep. Prog. Phys., 70, 1099
Omukai K., 2000, ApJ, 534, 809
Ouchi M. et al., 2008, ApJS, 176, 301
Padovani P., Matteucci F., 1993, ApJ, 416, 26
Palla F., Salpeter E. E., Stahler S. W., 1983, ApJ, 271, 632
Pirzkal N., Malhotra S., Rhoads J. E., Xu C., 2007, ApJ, 667, 49
Riechers D. A., 2011, ArXiv e-prints
Riechers D. A., Hodge J., Walter F., Carilli C. L., Bertoldi F., 2011, ApJ, 739, L31
Santos M. R., Ellis R. S., Kneib J.-P., Richard J., Kuijken K., 2004, ApJ, 606, 683
Saro A., Borgani S., Tornatore L., Dolag K., Murante G., Biviano A., Calura F., Charlot S., 2006, MNRAS, 373, 397
Shimasaku K. et al., 2006, PASJ, 58, 313
Solomon P. M., Vanden Bout P. A., 2005, ARA&A, 43, 677
Solomon P. M., Rivolo A. R., Barrett J., Yahil A., 1987, ApJ, 319, 730
Springel V., 2005, MNRAS, 364, 1105
Springel V., Hernquist L., 2003, MNRAS, 339, 312
Springel V., Yoshida N., White S. D. M., 2001, New Astron., 6, 79
Steidel C. C., Adelberger K. L., Shapley A. E., Pettini M., Dickinson M., Giavalisco M., 2000, ApJ, 532, 170
Sutherland R. S., Dopita M. A., 1993, ApJS, 88, 253
Tacconi L. J. et al., 2006, ApJ, 640, 228
Taniguchi Y. et al., 2005, PASJ, 57, 165
Todini P., Ferrara A., 2001, MNRAS, 325, 726
Tornatore L., Borgani S., Dolag K., Matteucci F., 2007, MNRAS, 382, 1050
Tornatore L., Borgani S., Viel M., Springel V., 2010, MNRAS, 402, 1911
Valiante R., Matteucci F., Recchi S., Calura F., 2009, New Astron., 14, 638
van den Hoek L. B., Groenewegen M. A. T., 1997, A&AS, 123, 305
Venemans B. P. et al., 2007, A&A, 461, 823
Verhamme A., Schaerer D., Maselli A., 2006, A&A, 460, 397

Wagg J., Kanekar N., Carilli C. L., 2009, ApJ, 697, L33
Walter F., Carilli C., Bertoldi F., Menten K., Cox P., Lo K. Y., Fan X., Strauss M. A., 2004, ApJ, 615, L17
Wang R. et al., 2010, ApJ, 714, 699
Weiß A., Downes D., Neri R., Walter F., Henkel C., Wilner D. J., Wagg J., Wiklind T., 2007, A&A, 467, 955

Wolfire M. G., McKee C. F., Hollenbach D., Tielens A. G. G. M., 2003, ApJ, 587, 278
Woosley S. E., Weaver T. A., 1995, ApJS, 101, 181

This paper has been typeset from a TEX/LATEX file prepared by the author.